

AceFF: A State-of-the-Art Machine Learning Potential for Small Molecules

Stephen E. Farr,[†] Stefan Doerr,[†] Antonio Mirarchi,[‡] Francesc Sabanés
Zariquiey,[†] and Gianni De Fabritiis^{*,‡,§}

[†]*Acellera Labs, C Dr Trueta 183, 08005, Barcelona, Spain*

[‡]*Computational Science Laboratory, Universitat Pompeu Fabra, Barcelona Biomedical
Research Park (PRBB), C Dr. Aiguader 88, 08003, Barcelona, Spain*

[¶]*Acellera, 38350 Fremont Blvd 203 Fremont CA, 94536 USA*

[§]*Institució Catalana de Recerca i Estudis Avançats (ICREA), Passeig Lluís Companys 23,
08010 Barcelona, Spain*

E-mail: g.defabritiis@gmail.com

Abstract

We introduce AceFF, a pre-trained machine learning interatomic potential (MLIP) optimized for small molecule drug discovery. While MLIPs have emerged as efficient alternatives to Density Functional Theory (DFT), generalizability across diverse chemical spaces remains difficult. AceFF addresses this via a refined TensorNet2 architecture trained on a comprehensive dataset of drug-like compounds. This approach yields a force field that balances high-throughput inference speed with DFT-level accuracy. AceFF fully supports the essential medicinal chemistry elements (H, B, C, N, O, F, Si, P, S, Cl, Br, I) and is explicitly trained to handle charged states. Validation against rigorous benchmarks, including complex torsional energy scans, molecular dynamics trajectories, batched minimizations, and tests of force and energy accuracy, demonstrates that AceFF is state-of-the-art for organic molecules in the accuracy and speed

regime important for drug discovery. The AceFF-2 model weights and inference code are available at <https://huggingface.co/Acellera/AceFF-2.0>.

1 Introduction

Atomistic simulations are fundamental tools for understanding materials and molecular systems at the atomic level. The accuracy and utility of these simulations critically depend on the choice of force field. Classical molecular mechanics (MM) force fields such as GAFF,^{1,2} CGenFF,^{3,4} OpenFF,^{5,6} and AMBER⁷ offer high computational efficiency, but often fall short in predictive accuracy, particularly for diverse, drug-like molecules containing rare functional groups or where quantum effects and polarization play significant roles. First-principles quantum mechanical (QM) methods, such as density functional theory (DFT), provide substantially higher accuracy but are prohibitively expensive for routine biomolecular simulations.

Machine learning interatomic potentials (MLIPs) offer a promising alternative, achieving near-QM accuracy at a fraction of the computational cost: an order of magnitude slower than MM methods, while being many orders of magnitude faster than QM approaches.⁸⁻¹¹ The current state-of-the-art MLIP architectures in terms of accuracy include equivariant message-passing graph neural network models such as MACE,¹² Nequip,¹³ AIMNet2,¹⁴ and TensorNet,¹⁵ to name a few.¹⁶ One of the most used models to date is ANI-2x,¹⁷ which employs a less accurate invariant architecture but is one of the most computationally efficient MLIPs available. A newer and more accurate group of pre-trained models are the MACE-OFF23 models with large, medium, and small variants available. These are significantly more accurate than ANI-2x, with the downside of being substantially slower.¹⁸ Other pre-trained models include: AIMNet2¹⁴ which supports charged molecules, AceFF-1.0¹⁹ based on the TensorNet architecture²⁰ supporting charge and spins, the Egret models, which are based on the MACE architecture,²¹ the recent OrbMol,²²⁻²⁴ and UMA-OMol25 models.²⁵

OrbMol and UMA are both trained on the recent OMol25 dataset²⁵ and cover most of the periodic table, while being accurate in standard benchmarks, they are slow relative to more specialized models. A recent fast model is SO3LR²⁶ which incorporates semi-local interactions from an equivariant neural network with universal pairwise force fields designed for short-range repulsion, long-range electrostatics, and dispersion interactions.

It is currently not feasible to perform production MD using a full MLIP description of the entire molecular system. Instead, it is necessary to use hybrid MLIP/MM schemes, where only the ligand is modeled with the MLIP, and the remainder of the system uses a classical MM force field. It has been found that even with a simple mechanical embedding approach, MLIP/MM can provide increased accuracy for RBF E calculations.^{27,28} In our previous work, we were limited by the fact that ANI-2x supports only eight elements and only neutral molecules. This led us to create our own QM dataset and develop our first MLIP, AceFF-1.0,¹⁹ which we applied in a large-scale RBF E benchmark, finding improved accuracy compared to traditional force fields and previous ANI-2x results.²⁸ AceFF-1.1 included a larger dataset and was released on HuggingFace.²⁹ Both of these models are freely available under the Apache 2.0 license for academic and commercial use. In this paper, we report the latest update to our model family, AceFF-2, which includes both more training data and an improved model architecture, TensorNet2, and a faster implementation with optimized Nvidia warp kernels. Additionally, we describe the various benchmarks we use to quickly assess model accuracy, making comparisons in accuracy with the existing MLIPs ANI-2x,¹⁷ AIMNet2,¹⁴ OrbMol,^{22,23} UMA,²⁵ semi-empirical methods g-XTB,³⁰ GFN2-XTB,³¹ and the MM forcefield GAFF2.^{1,2} In summary, AceFF-2 is one of the fastest models with high accuracy, because of this, we believe that it has immediate applications in drug discovery.

2 Results

2.1 TensorNet2 architecture

AceFF-1.x models were based on TensorNet¹⁵ models with charge and spin encodings.²⁰ With AceFF-2, we introduce a modified version of TensorNet with improved charge handling. The approach we take closely follows that of AIMNet2:¹⁴ we include additional scalar features to mimic partial charges, perform neutral charge equilibration on them, and use them in a long-range Coulomb energy term. We name this version TensorNet2. An overview of the model architecture is shown in figure 1.

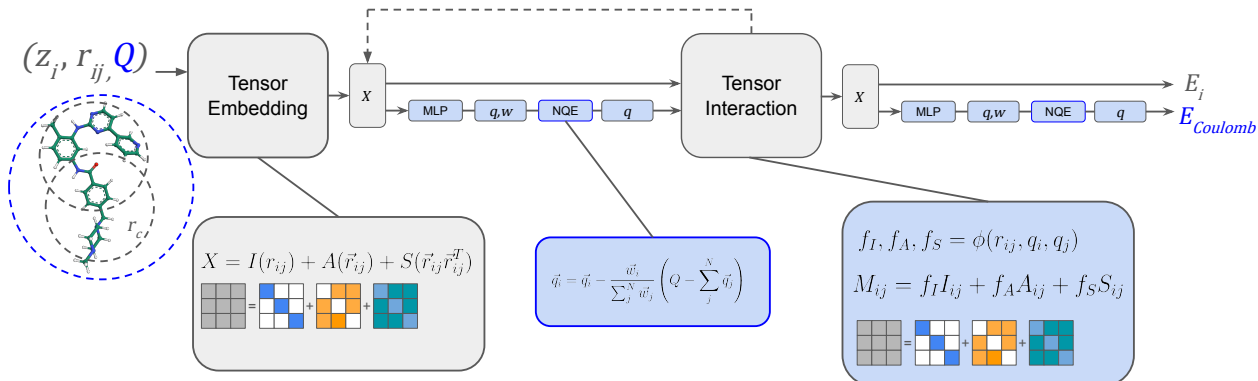


Figure 1: The AceFF-2 architecture TensorNet2 builds upon TensorNet¹⁵ with the new components colored in blue. The main change is that after the tensor embedding, and each tensor interaction block, a set of partial charges q and weights w are computed and undergo a neutral charge equilibration (NQE) procedure as done in AIMNet2.¹⁴ The partial charges are then combined with edge features during the tensor interaction. The predicted charges are used to compute a Coulomb energy E_{Coulomb} alongside the standard short range node-wise MLIP energy term E_i . The dashed arrow represents where iteration occurs for more than one interaction layer. The pictured diagram corresponds to TensorNet2 1-layer. The grey dashed circles around the example molecule illustrate the short cutoffs used in the tensor embedding and interaction. The blue dashed circle represents the long range of the total charge (a global feature feature), NQE block, and the Coulomb interaction.

From an input of atomic numbers and coordinates Z_i, R_i , TensorNet learns a set of 3×3 matrices (rank-2 tensors) for each atom $X^{(i)}$ which are equivariant to rotation and translation. At each message-passing step, the $X^{(i)}$ are updated based on the neighboring atoms,

making use of the fact that $X^{(i)}$ can be decomposed into scalar, vector, and symmetric traceless components, I , A , S , respectively. After several message passing updates, the squared Frobenius norms of the representations, which are invariant under $O(3)$, are further processed by the neural network to predict energies, obtaining atomic forces via automatic differentiation. Moreover, a distinctive feature of the TensorNet message-passing architecture, specifically when interaction layers are active, is its natural transition from $O(3)$ to $SO(3)$ equivariance. This reduction in symmetry follows directly from how tensor-tensor interaction products are computed in the interaction layer, which mix even and odd parities and therefore break reflection equivariance while preserving full rotational equivariance. This behavior is especially valuable in drug discovery, where chirality is central: enantiomers are related by reflections but often differ dramatically in binding affinity and biological activity.³²

In the previous version of TensorNet,²⁰ total molecular charge Q was included in a simple manner with no extra learned parameters. While this method effectively resolved the degeneracy problem for molecules sharing the same coordinates and atomic numbers but differing in Q , we observed limitations during extrapolation. Specifically, when tested on a set of larger charged molecules, the performance was significantly surpassed by the AIMNet2 architecture,¹⁴ which explicitly models and learns partial charges and Coulomb interactions.

We incorporate the AIMNet2-like neutral charge equilibration into TensorNet as follows, which is the main contribution to TensorNet2 new architecture. At each message passing layer, we introduce a charge prediction neural network that accepts the node features (I^i, A^i, S^i) as input and outputs a set of charge predictions (\vec{q}_i) and a corresponding set of weights (\vec{w}_i) . It is important to note the inclusion of a feature dimension (a hyperparameter) to increase expressivity. These outputs are not required to represent physical charges but rather scalar features that we equate to partial charge hypotheses (similar to the approach in³³). A neutral charge equilibration step is then performed independently across each feature channel to ensure that the partial charges sum to the total molecular charge (Q).

$$\vec{q}_i = \vec{q}_i - \frac{\vec{w}_i}{\sum_j^N \vec{w}_j} \left(Q - \sum_j^N \vec{q}_j \right), \quad (1)$$

which is the same as in.¹⁴ The q_i from each node are then used in the next message passing update by extending the scalar edge features such that Equation 11 in¹⁵ becomes:

$$f_I^i, f_A^i, f_S^i = \phi(r_{ij}) \text{SiLU} \left(\text{MLP} \left(e^{\text{RBF}}(r_{ij}) \oplus q_i \oplus q_j \right) \right), \quad (2)$$

where \oplus denotes tensor concatenation. The predicted \vec{q}_i from all layers are subsequently used to compute Coulomb interactions, which is performed independently across each feature channel. The weighted mean of the resulting Coulomb energy is then calculated, where the weights are assigned such that the output from the final layer has the most significant impact on the total energy. Utilizing the charge predictions from the earlier layers in the final output calculation effectively serves as a regularization technique.

This procedure constitutes a type of self-consistent method and is fundamentally different in style from alternative charge inclusion techniques such as the latent Ewald summation method,³⁴ which calculates an Ewald summation or a Coulomb-like interaction using node features derived from just the final node features. Another is the 4G-HDNNP approach,³⁵ which employs neural networks to predict electronegativity and hardness. This prediction is followed by a full charge equilibration scheme, which involves solving a set of linear equations to find the set of partial charges that minimizes the electrostatic energy subject to the total charge constraint, which scales poorly with system size. The TensorNet2 neutral charge equilibration approach adds only a small overhead to training and inference speed. For example, a 1-layer TensorNet model with an embedding dimension of 128 and 32 radial basis functions has 535,681 parameters, while a 1-layer TensorNet2 model with the same embedding dimension, radial basis functions, and additionally a charge dimension of 16 has 685,413 parameters. The inference speeds of each model for a 1500 atom system (500 water molecules) are 100 steps/second and 75 steps/second, respectively. A parameter increase of

28% and a speed decrease of 25%.

2.2 Software Optimizations

With this model update, we have introduced software optimizations to the TensorNet models within the TorchMD-Net³⁶ package. These optimizations utilize custom NVIDIA warp kernels, implemented from the MatGL package,^{37,38} for the primary bottleneck operations: the decomposition and composition between the X and I, A, S tensors, as well as the message-passing routines. This implementation results in a 3x speed-up for both inference and training. Figure 2 illustrates the molecular dynamics inference speed (time per step) as a function of system size, comparing the legacy code to the optimized version. The updated code also

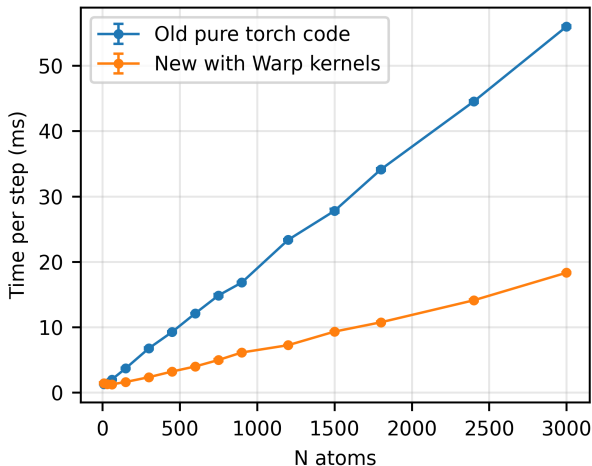


Figure 2: Molecular dynamics speed (time per step) for increasing number of atoms. The blue line is the old pure PyTorch version of TensorNet and the orange line is the new version using the Warp kernels available in TorchMD-Net version 3. These timings are both for the same TensorNet 1 layer model

achieves a 3x reduction in GPU memory usage. These improvements stem from a more efficient representation of the I, A, S tensors. The original implementation stored these as three separate 3×3 tensors to facilitate PyTorch vectorization. Mathematically, however, $I, A,$ and S represent a scalar, a vector, and a symmetric traceless tensor, which can be represented by 1, 3, and 5 values, respectively. The new optimized kernels maintain this compact

format throughout, eliminating the overhead of expanding to 3×3 tensors populated with zero entries. Furthermore, the message passing kernels avoid the creation of large edge sized intermediate tensors are required for Autograd.

2.3 AceFF-2 trained model

We trained a 2-layer version of TensorNet2 on an internal QM dataset. We used a charge embedding dimension of 16, a hidden dimension of 128, and 32 radial basis functions. The model was trained using the torchmd-train scripts that can be found in TorchMD-Net.³⁶ We refer to this model as AceFF-2. The model was trained on energy and force labels, without using any partial charge or dipole moment data. Optionally, one of the TensorNet2 charge channels could be trained on a QM level specific type of partial charge, e.g. MBIS, to facilitate an approach such as.³⁹ Indeed, we expect the different charge channels could be trained simultaneously on multiple QM-derived partial charges—for example, the Omol25 dataset contains Mulliken and Lowdin charges.²⁵ For ablation purposes, we also trained a 1-layer version with all other hyperparameters unchanged.

2.4 Accuracy on torsion scans

The first benchmark test we performed was Sellers et al torsion scan.⁴⁰ This benchmark data set contains torsion scans of 62 molecules done with different levels of QM. We take the most accurate method from the set, CCSD(T)/CBS, and use this as the reference to compare against. For all molecules in the test, we performed relaxed torsion scans (as done in^{41,42}). For comparison we did the same procedure with our AceFF-1.0, ANI-2x¹⁷ from torchani,⁴³ AIMNet2,¹⁴ and the recent OrbMol-conservative.²²⁻²⁴ We also did the scan with the semi-empirical method GFN2-XTB⁴⁴ and the molecular mechanics force-field GAFF.^{1,2} We excluded g-XTB because it does not have analytical gradients available yet. The MAE of each torsion scan relative to the reference scan is plotted in 3a as box-plots with all data points shown. We see that OrbMol is the most accurate model, with AceFF-2 a close second.

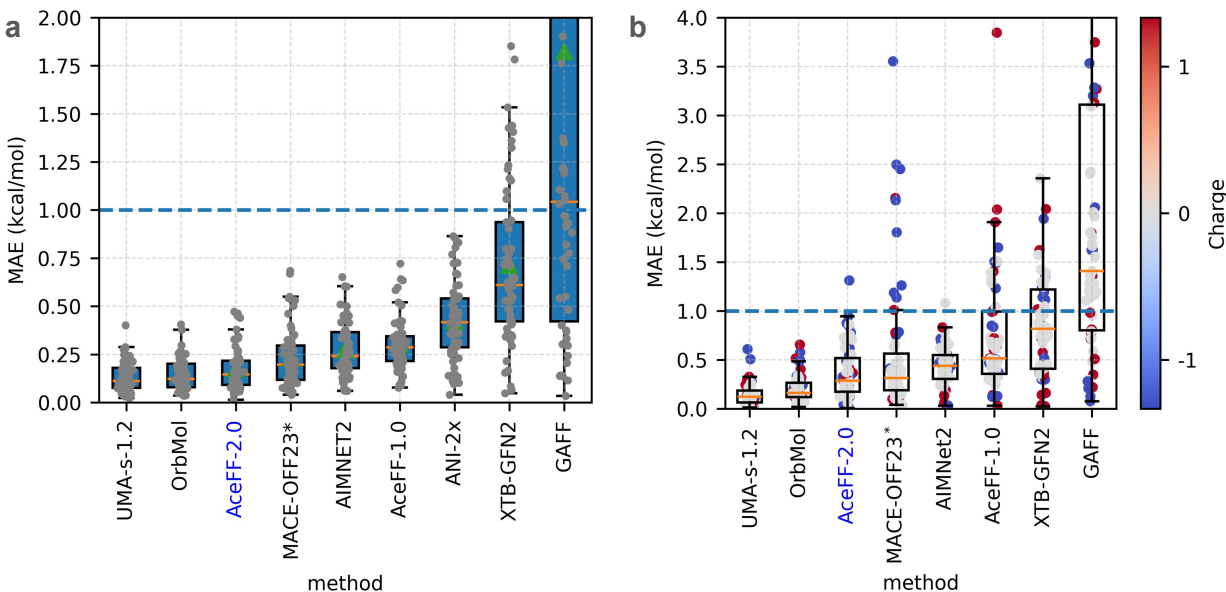


Figure 3: Torsion scans. **a.** Sellers et al. torsion scan benchmark.⁴⁰ The orange lines are the median value. The methods are ordered from left to right by median MAE compared to the coupled cluster reference data. The y-axis has been intentionally capped at 2.0 kcal/mol to focus on the differences between the MLIP models. An image of one of the molecules with the torsion angle indicated is pictured. Values marked by * were taken from a previous publication.²⁸ All other data points were recalculated. **b.** Behara et al torsion scan benchmark.⁴⁵ The orange lines are the median value. The methods are ordered from left to right by median MAE compared to the coupled cluster reference data. The scatter points are color-coded by the molecular charge. The y-axis has been intentionally capped at 4.0kcal/mol to focus on the differences between the MLIPs. Data points of methods marked with * were taken from the original data,⁴⁵ all other data points were recalculated. On both plots, a guide line has been drawn at 1 kcal/mol.

From left to right, the other MLIPs perform similarly until ANI-2X, which is significantly worse. GFN2-XTB performs poorly compared to the MLIPs, and as expected, GAFF has very large errors.

We also performed a second torsion scan benchmark from Behara et al.⁴⁵ This torsion scan contains charged molecules, specifically $[0,-1,+1]$. The reference torsion drives were done with MP2/heavy-aug-cc-pVTZ, and the reference single point energies were labeled with CCSD(T)/CBS. The benchmark differs from the Sellers et al torsion scan in that we do not perform any geometry optimizations. This benchmark tests only the energy error of the MLIP and not the force calculations. We did the single point calculations for OrbMol,

AceFF-2, AceFF-1.0, AIMNet2, GFN2-XTB, and GAFF. We took the single point results for MACE-OFF23 from⁴⁵ for extra comparison.

The MAE of each method is plotted in figure 3b. The trend between models is approximately the same as the Sellers et al torsion scan. As expected, the biggest outliers in AceFF-1.0 are the charged molecules, and similarly for MACE-OFF23 which was designed for only neutral molecules. While UMA, OrbMol, and AceFF2 demonstrate a more balanced performance across both neutral and charged molecules, charged species still represent the most significant deviations for all three. Notably, AIMNet2 is the only model where the largest outlier is a neutral molecule.

2.5 Accuracy on strained conformers: Wiggle150

The Wiggle150 benchmark⁴⁶ consists of 150 highly strained conformations of adenosine, benzylpenicillin, and efavirenz, with reference energies calculated using DLPNO-CCSD(T)/CBS level of theory. To evaluate performance, we used the MLIP model to predict the relative energies (relative to the minimized geometry) for all 150 conformations. The resulting mean absolute error (MAE) and mean absolute deviation (MAD) were then computed compared to the reference values.

Table 1 summarizes the Wiggle150 results for ANI-2x, g-XTB, AceFF-1.0, AceFF-2, AIMNet2, OrbMol, and UMA-s-1.2. Data for ANI-2x, AIMNet2, and GFN2-XTB was taken from the original Wiggle150 publication,⁴⁶ while the remaining values were computed in-house using their respective publicly available models. OrbMol and UMA exhibit the highest accuracy. Notably, all MLIPs (excluding ANI2x) outperform the semi-empirical g-XTB method, despite g-XTB being designed to achieve a similar chemical accuracy level (ω B97M-V). Furthermore, AceFF-2 shows a significant improvement over AceFF-1.0.

Table 1: Performance of MLIPs, and one semi-empirical method, and one MM force-field on the Wiggle150 benchmark⁴⁶

Method	MAE (kcal/mol)	RMSE (kcal/mol)
GAFF	22.87	30.86
GFN2-XTB	14.6	15.2
ANI-2X	4.41	5.41
g-XTB	3.85	4.76
AceFF-1.0	2.73	3.32
AIMNet2	2.39	3.13
AceFF-2	1.76	2.34
UMA-s-1.2 (omol task)	0.92	1.23
OrbMol	0.89	1.22

2.6 Drug-like molecules: Schrödinger ligands

We created a test set that evaluates how well the model generalizes to larger, previously unseen molecules. These ligands are all larger than 30 atoms, which is the maximum size included in the AceFF DFT training dataset. To create the Schrödinger ligand test set, we took the ligand structures from⁴⁷ available at https://github.com/schrodinger/public_binding_free_energy_benchmark and labeled them with forces and energies computed at the AceFF level of theory (ω B97M-V/def2-TZVPPD). All ligands from the Merck, JACS, and charge-annil sets were included. We used the conformations directly from the provided SDF files and performed DFT calculations with the same settings used to create the AceFF DFT dataset. Any conformations that failed to converge were discarded, resulting in a final set of 650 conformers. We predicted the force and energy using AceFF-1.0, AceFF-2, AIMNet2, OrbMol, and UMS-s-1.2. For each method, we computed the force MAE per conformer and the energy absolute error. It is important to note that the energy is the total DFT energy; as such, we only expect the AceFF models, which are trained on the same level of theory DFT, to have energy errors close to zero. The AIMNet2, OrbMol, and UMA models were trained on data generated by slightly different functionals, basis sets, and software. However, the force errors should be comparable between the models, as this is an intrinsic physical property. Therefore, we only show energy errors for the AceFF models.

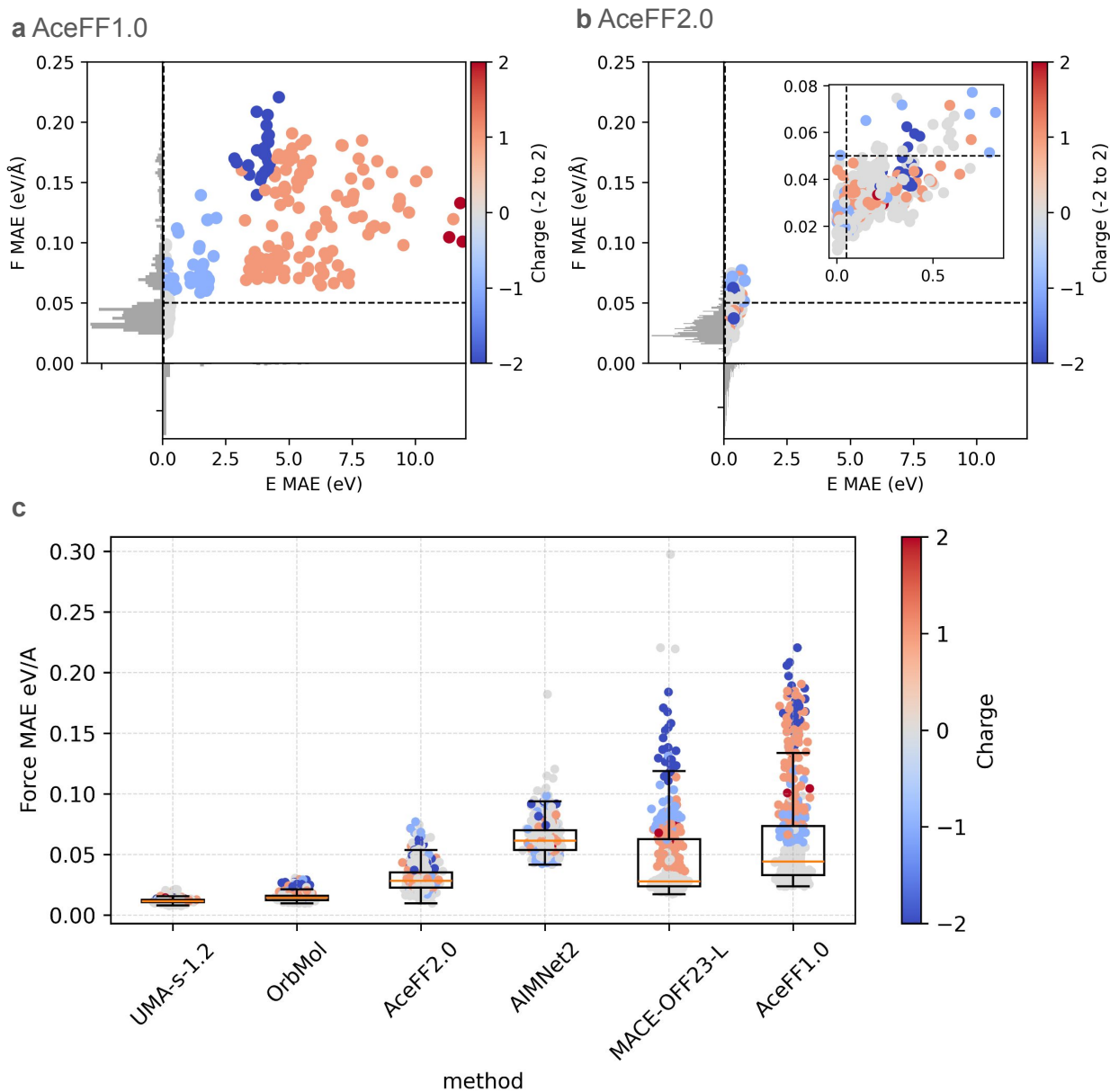


Figure 4: Schrödinger ligand test set evaluation. **a.** Energy error vs force error for AceFF-1.0, color-coded by ligand total charge. **b.** Energy error vs force error for AceFF-2, color-coded by ligand total charge. The axis range is the same in sub-plots a and b to aid comparison. The inset graph in sub-plot b shows a zoomed-in view of the data points. **c.** Force errors for all tested models. The orange line is the median value. The data points are color-coded by charge.

The results are plotted in Figure 4a and 4b for AceFF-1.0 and AceFF-2, respectively, showing the force and energy errors. We have plotted guide lines at $0.05\text{eV}/\text{\AA}$ and 0.05eV , which indicate the approximate validation L1 force and energy loss that the models converge to. We see that, as expected, AceFF-1.0 performs very badly on charged molecules. AceFF-2 performs much better with the majority of force errors below $0.05\text{eV}/\text{\AA}$. The energy errors are not below 0.05 eV ; however, these molecules are mostly larger (range of 27 to 74 atoms) than any it was trained on.

The force errors for all models are plotted in figure 4c. AIMNet2 has consistent performance between charged and neutral molecules, but is systematically above $0.05\text{eV}/\text{\AA}$. UMAS-1.2 performs exceptionally well with force errors all below $0.02\text{eV}/\text{\AA}$, closely followed by OrbMol which has all errors below $0.03\text{eV}/\text{\AA}$. We note that both OrbMol and UMAS-1p2 were trained on the OMol25 dataset, which does contain molecules of this size (and may well contain these molecules or very similar ones in the training split). It is interesting to see that the most extreme outliers for AIMNet2 are neutral molecules.

2.7 Potential energy smoothness

A smooth potential energy surface is crucial for stable molecular dynamics simulations. To assess model smoothness, we analyzed the potential energy scan as the C-C bond in an ethane molecule was compressed and extended. We compressed the bond to an unphysically small distance and extended it beyond the bond-breaking regime to examine how the MLIPs behave in these regions outside the training domain. We compared the MLIP results with those from DFT using $\omega\text{B97m-V}/\text{tzvppd}$. The bond energy scans are plotted in Figure 5, where they have all been shifted such that the minimum energies are zero.

All models exhibit similar behavior in the minima. At small distances, we observe the nuclear repulsion in the DFT curve, with the same feature visible in the OrbMol curve (notably, this model includes a ZBL repulsive term). For the other MLIPs, the nuclear repulsion is modeled entirely by the neural network terms (and the data upon which they

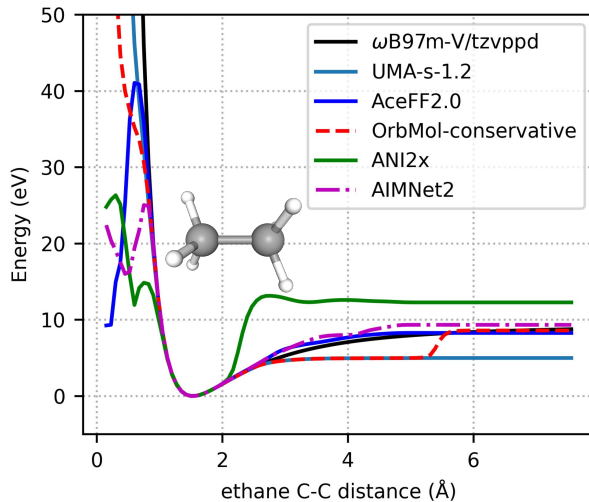


Figure 5: Potential energy of ethane C-C bond length scan for different MLIPs compared to a reference of DFT with ω B97m-V/tzvppd.

were trained). The energy barrier in ANI2x is less sharply defined. In contrast, the AceFF-2 energy matches the DFT energy up to a large energy of 40 eV. At the bond-stretching end of the curve, we observe that ANI2x significantly overestimates the bond strength, UMA-s-1.2 underestimates it, and OrbMol exhibits an unphysical step change between 5 and 6 Å, which is perhaps an artifact of the MLIP cutoffs. AIMNet2 and AceFF-2 have similar profiles to each other and to the DFT reference, these two models are the only ones that include a long range coulomb term which enables atom interactions beyond the typical graph cutoff (5 Å to 6 Å).

2.8 Inference speed scaling with molecular dynamics

We compared model speed by running molecular dynamics on water boxes of increasing size. When running MLIPs in this way, it is possible to turn on aggressive compilation settings because certain tensors will have fixed shapes and/or values, e.g. the number of atoms will be constant, the number of edges can be set to a constant, and the atomic numbers will always be the same. We used the Atomic Simulation Environment⁴⁸ (ASE) calculator implementations of each model. For OrbMol, `compile=True` is used; for AceFF models, we

use `torch.compile(mode='reduce-overhead')`, which enables CUDA graphs; for ANI-2x, we use the `cuaev` extension from the latest TorchANI2.0;⁴⁹ for the MACE-MPA-0 model, we used CuEquivariance plugin; and for AIMNet2, we used both the official torch-scripted models and our modified version that is compatible with `torch.compile` and CUDA graphs. These are the fastest settings that the models currently have available.

In this work, we are primarily concerned with simulating small drug-like molecules or a small MLIP/MM region of a protein ligand complex. No models are currently fast and accurate enough for a full system bio-molecular simulation ($> 10,000$ atoms) of any useful timescale. Therefore, we restricted our speed testing to a limit of 3000 atoms (1000 water molecules).

The steps per second of all models as a function of system size is shown in Figure 6. An important point to note is that only AceFF and AIMNet2-CUDA graphs utilize CUDA graphs, which are essential for low latency in small systems.³⁶

There is a clear latency limit for less than 300 atoms for all models except AceFF and AIMNet2-CUDA graphs — the CUDA graph compatibility explained before is the primary reason they can reach speeds faster than 100 steps/second. OrbMol, ANI, and standard AIMNet2 are all limited to >10 ms latency, while the MACE-MPA-A, and UMA models have even larger latency limits. Once N is large enough, the models scale as expected: Orb, AceFF-1.0, and MACE are linear; AceFF-2 and AIMNet2 are quadratic (due to their N^2 Coulomb interaction implementations). ANI2X appears to have no clear speed decrease and is limited by latency for all N we are looking at. This follows the speed scaling reported in TorchANI2.0,⁴⁹ where much larger system sizes are reached.

We also tested the speed of batched molecular dynamics. To do this, we selected a small molecule (imatinib, 68 atoms) and generated N conformers. We then ran Langevin dynamics, using the integrator from TorchMD,⁵⁰ in a batched manner, such that all N conformers were integrated simultaneously. TorchMD is a molecular dynamics engine entirely written in PyTorch, which allows for easy integration and batching of molecular simulations using MLIPs

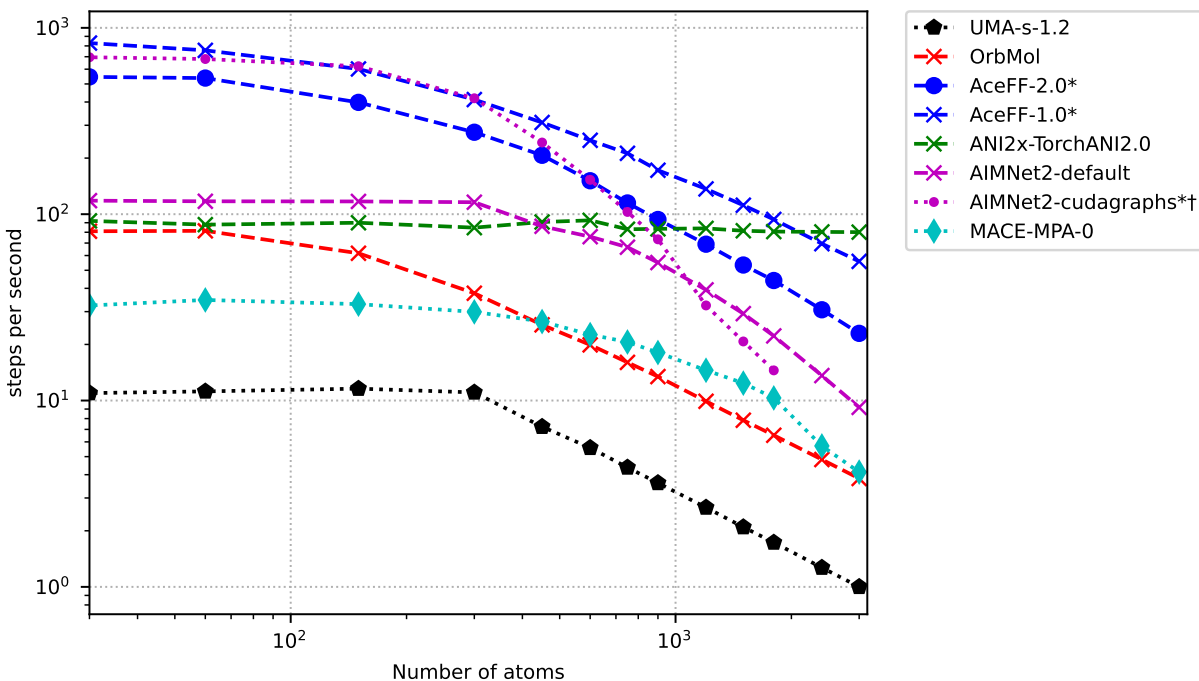


Figure 6: Inference speed in steps per second for different models vs number of atoms. Methods marked with an * have been run with CUDA graphs enabled. AIMNet2-CUDA graphs marked with † runs out of memory with more than 1500 atoms. This is due to the N^2 implementation of the CUDA graph-compatible code version.

and the Amber potential. This allowed the AceFF MLIP to be called once per timestep for the entire batch. The total time per step is plotted in figure 7a for increasing batch size. We compare against the serial OpenMM simulation speed, i.e., the time to sequentially run a timestep for each conformer individually. We also compute the effective total throughput in ns/day for the batched simulations, comparing against the OpenMM simulation throughput of running a single simulation. These results are plotted in figure 7b. We see that for 32 conformers there is almost a 10x increase in the total simulation throughput, this is due to the latency limits of running a full forward+backwards pass being overcome.

2.9 MLIP/MM molecular dynamics stability and speed

A current use-case for MLIPs is in mixed MLIP/MM simulations where a small region is modeled with the MLIP and the rest of the system with a traditional MM forcefield. [27,28,51](#)

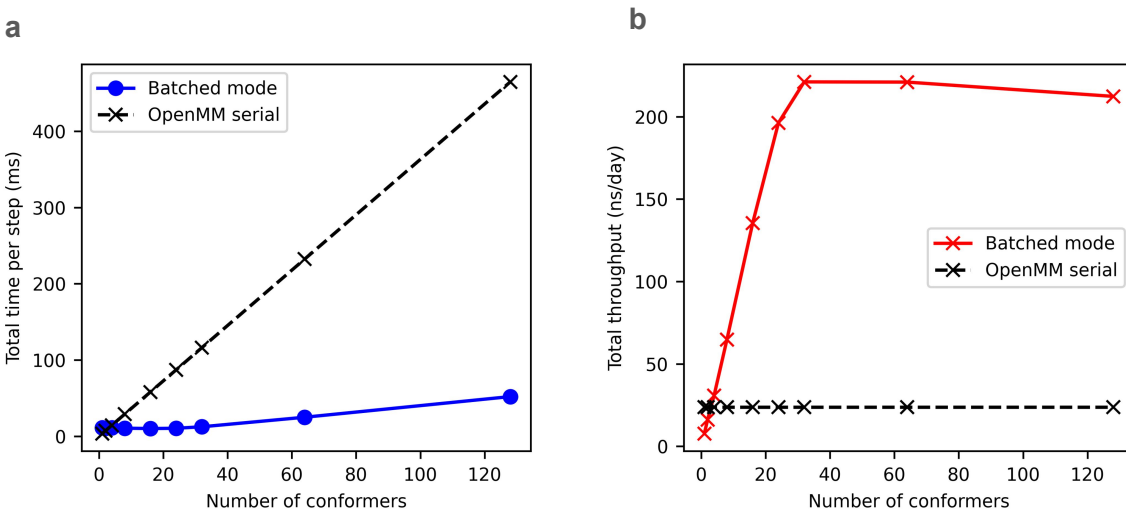


Figure 7: Batched molecular dynamics with AceFF-2. **a.** The total time per step for the corresponding number of conformers in batched mode (blue line) and in serial with OpenMM (black line). **b.** The effective total throughput in ns/day for batched mode (red line) and using in serial using OpenMM (black line).

The simplest approach is the mechanical embedding approach, where just the ligand intramolecular forces are computed with the MLIP and the rest of the system uses the MM forcefield. This accounts for the corrections due to ligand strain.

To test that AceFF-2 is appropriate for this, we ran a simulation of the ejm31 ligand bound to Tyk2, which is one of the systems studied in²⁸ and from⁴⁷ the complex is shown in figure 8a. We used the OpenMM-ML package⁵² to run the simulations with HMR of 4au, temperature of 300K, and a Langevin thermostat. We ran the simulations for 100ns with a timestep of 1fs and a timestep of 2fs. The ligand RMSDs are plotted in 8b and the center of mass distance between the ligand and protein pocket are plotted in 8c. We observe that both 2fs and 1fs are stable. The simulation speeds on an RTX4090 are 36.7 ns/day and 72.6 ns/day, respectively. We also tested the speed of the same simulation using AceFF-1.0, ANI2x, and MACE-MPA-0 using the implementations available in OpenMM-ML. The speeds for the tested models are shown in table 2 for simulations run with a 1fs timestep.

We see that the AceFF-1.0 speed of 63.8ns/day is slightly faster than the ANI-2x speed of 59.1 while it is significantly faster than the MACE model. AceFF-2, which includes an

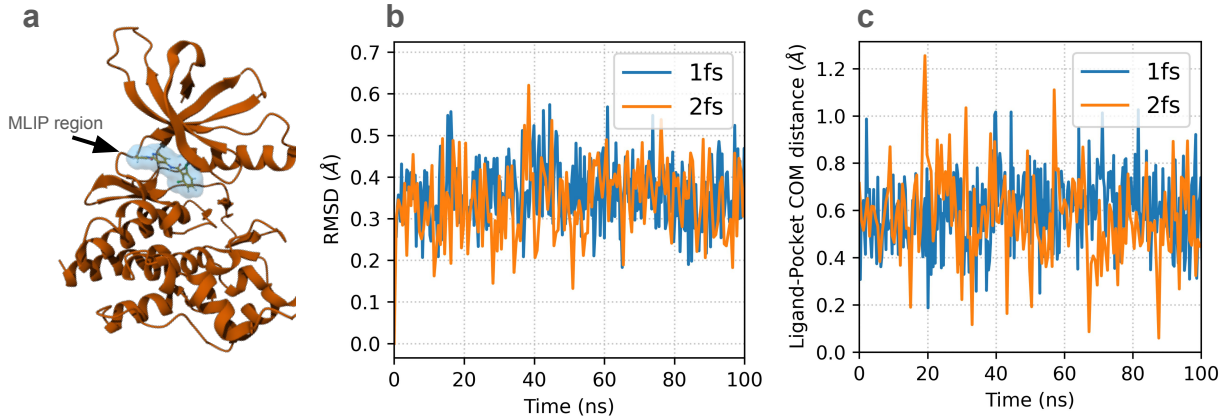


Figure 8: Ligand RMSD of NVT molecular dynamics of protein-ligand complex using ML/MM. **a.** Visualization system, the MLIP region has been highlighted and water has been omitted for clarity. **b.** The RMSD of the ligand is plotted for the 1fs and 2fs timestep AceFF-2 simulations in blue and orange, respectively. **c.** The ligand-pocket center of mass distance is plotted for the 1fs and 2fs timestep AceFF-2 simulation in blue and orange, respectively.

Table 2: Simulation speed of a MLIP/MM using OpenMM-ML with a 1fs timestep. AceFF models marked with a * utilize CUDA graphs

	Speed on a RTX4090 (ns/day)
ANI-2x	59.1
AceFF-1.0*	63.8
AceFF-2*	36.7
MACE-MPA-0	4.2

additional message-passing layer, charge prediction heads, and explicit Coulomb terms, is less than a factor 2 slower than AceFF-1.0. It is important to note that only the TensorNet-based AceFF models are compatible with CUDA graphs (and have CUDA graphs enabled in this test), which we have previously found is essential for low-latency simulations. The code changes to make a model CUDA graph compatible are non-trivial. Additionally, to interface seamlessly with OpenMM for MLIP/MM simulations, a model must be implemented in the OpenMM-ML package. Currently, only ANI-2x and MACE implementations have been released. Since OpenMM-ML strictly requires TorchScript compatibility, we cannot test the OrbMol model without making non-trivial code changes.

2.10 Batched conformer minimization

A common use case of molecular force fields is to energy minimize molecular conformations. To assess the ability of the MLIPs to minimize a diverse array of molecules relevant for drug discovery, we tested them on the Platinum Diverse dataset,⁵³ which contains 2859 crystallographic structures of ligand conformations from protein ligand complexes.

To perform the benchmark, we took the reference conformer from the dataset and minimized it with the MLIP. It is expected that the minimization should converge, and that the reference structure is close to a local minima of the MLIP force field, such that after minimization, the RMSD between the reference and the minimized structure should be small. We tested AceFF-2, AIMNet2, and OrbMol; and excluded ANI2x due to the large number of charged molecules present in the dataset and elements outside the ANI2x subset. For this test, we used the ASE LBFGS minimizer and the ASE calculator interfaces of the MLIP models.

The number of failed minimizations and the values for the RMSD mean, median, and percentages under 1Å, 2Å, 3Å, and 10Å are shown in table 3. The histograms of the RMSDs are shown in figure 9. For consistent comparison, the mean, median, and standard deviation are taken over molecules where all methods succeeded (N=2850).

For AceFF-2, we found that two molecules failed to minimize, resulting in unphysical “exploded” structures. These are molecules with index 1653 (name: GVF_2UVM_L) and index 1816 (name: JD5_4NFK_F). Molecule 1653 has a net charge of -8 due to four -2 phosphate groups; similarly, molecule 1816 has a net charge of -3 and two phosphate groups. Images of these molecules are shown in figure 9b and 9c. The AceFF dataset contains molecules with net charge up to -2 to 2, so these specific molecules are significantly outside the domain of knowledge of the model, and it is not surprising that it fails to correctly model them. The next largest RMSD is 3.9 angstrom for molecule 1928, while not exploded, the conformation is in an elongated state compared to the reference and an H atom has changed bond topology. This molecule has a net charge of -4, so once again outside the training

Table 3: Platinum Diverse geometry optimization benchmark results. The summary values describe the RMSDs between the initial reference structure and the geometry-optimized structure for the three tested MLIPs. The statistics are taken over the subset where all methods had no failures (N=2850).

MLIP	mean	std	median	%<1Å	%<2Å	%<3Å	%<10Å	Number failed
AceFF-2	0.552	0.446	0.419	86.29	98.43	99.72	99.93	2
AIMNet2	0.508	0.426	0.388	89.75	98.60	99.62	99.72	8
OrbMol	0.534	0.432	0.400	86.92	98.64	99.86	100.00	0

domain. An image of this molecule is shown in figure 9d.

For AIMNet2, we found that 8 molecules exploded with RMSDs greater than 10. The molecule indexes are [259, 1160, 1468, 1648, 1816, 2189, 2328, 2803], all contain the same large net charge and phosphate groups that AceFF struggled with.

OrbMol succeeds at minimizing all conformers; this can be attributed to its much larger and diverse training dataset (OMol25 is an order of magnitude larger than AceFF-2 and AIMNet2 datasets). AIMNet2 has the smallest mean and median, suggesting its local minima are the closest to the reference geometries. Looking at the distributions, we see no major differences. Two-sided Kolmogorov-Smirnov test (N=2850) between the three pairs is: AceFF-2 vs AIMNet2: statistic=0.0505, p-value=0.00138; AceFF-2 vs OrbMol: statistic=0.0347, p-value=0.0642; AIMNet2 vs OrbMol: statistic=0.0368, p-value=0.0418. Therefore, the AceFF-2 and OrbMol results are not significantly different, while the AIMNet2 results have a maximal difference of 5%. Orb and AceFF-2 are trained on the same level of DFT, so this is expected. An important point to note is that the reference geometries are from protein-ligand complexes; the in-vacuum local minima that the MLIPs are optimizing to will be different from the bound minima.

We also assessed the speed of optimizing multiple conformers. The benefit of MLIPs is that batching calculations is trivial using the existing optimizers available in PyTorch. Helpfully, LBFGS, one of the standard methods for geometry optimization, is available. We recorded the time taken to minimize N conformers of Imatinib, a drug molecule with

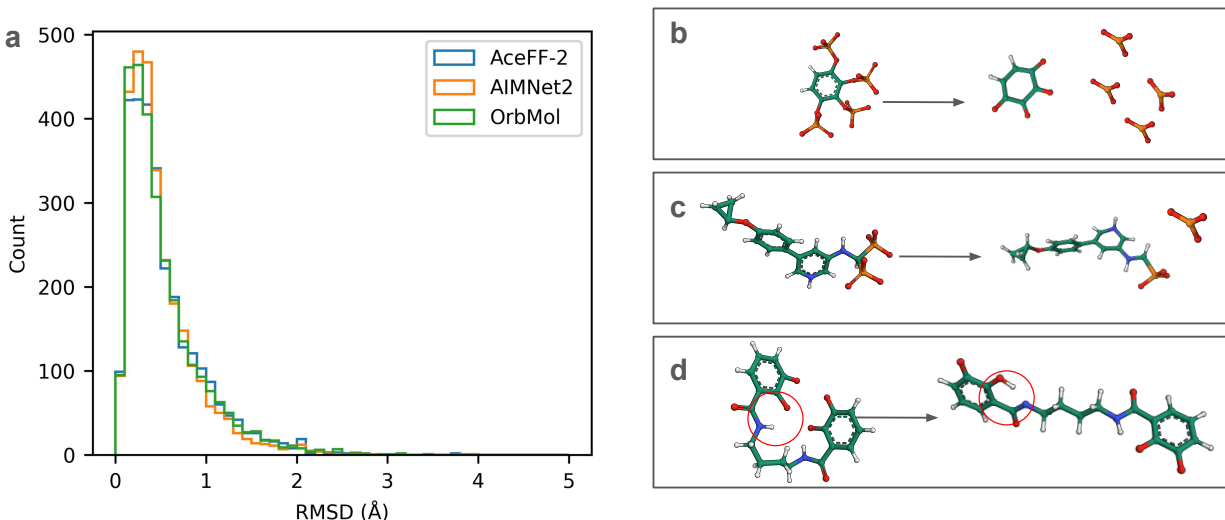


Figure 9: Platinum Diverse geometry optimization benchmark. **a.** The histogram of the RMSDs between the initial reference structure and the geometry-optimized structure for the three tested MLIPs for all conformers in the Platinum Diverse set.⁵³ **b.** Molecule index 1653 has a net charge of -8 due to four phosphate groups. When minimized with AceFF-2 the phosphates are ejected. **c.** Molecule index 1816 has a net charge of -3 and two phosphate groups, when minimized with AceFF-2 one of the phosphates is ejected. **d.** Molecule index 1928 has the largest RMSD (3.9 Å) for AceFF-2, it has a net charge of -4, upon minimization with AceFF-2 there is a change in bond topology as highlighted by the red circles.

68 atoms.⁵⁴ We varied N from 1 to 100 and put all conformers into the same batch. For comparison, we timed ASE LBFGS minimization (for the same number of steps, in this case 400) for one conformer, and scaled this linearly by N to get the ASE serial speed baseline. The measured timings are shown in Figure 10. The batched speed is significantly faster for more than 20 conformers. In the supplementary information, we verify that LBFGS from PyTorch correctly minimizes atomic configurations in a comparable way to ASE’s LBFGS. For fewer than 10 conformers, the ASE version is faster because it utilizes torch.compile and CUDA Graphs to minimize execution latency. Conversely, the batched version used with torch.optim does not employ CUDA Graph settings. We have provided an investigation of speed scaling across various torch.compile configurations in the Supplementary Information.

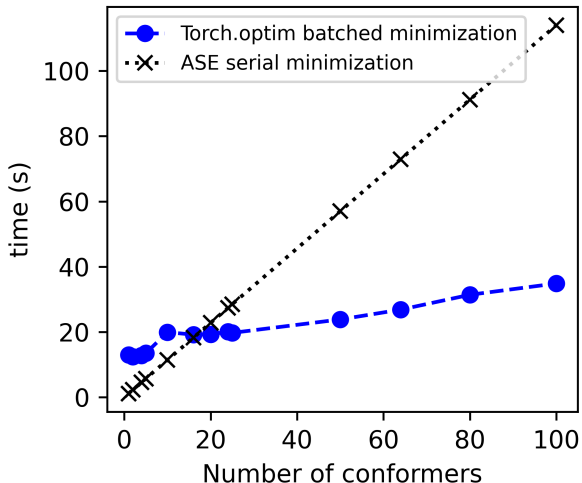


Figure 10: Comparison of batched conformer minimization speed with torch.optim.LBFGS and ASE serial minimization of the same number of conformers of an Imatinib molecule.

3 Conclusion

We have presented AceFF-2, a next-generation neural network potential tailored for the efficient and accurate simulation of small drug-like molecules. Building upon a robust DFT dataset, this model leverages the TensorNet2 architecture with charge embedding to deliver near-quantum mechanical accuracy while maintaining the speed required for routine molecular dynamics workflows.

We evaluated AceFF-2 using a comprehensive set of benchmarks, comparing it against other MLIPs and traditional methods. In the current MLIP landscape, ANI-2x¹⁷ represents one extreme, offering the fastest speed but with limited elemental coverage and restriction to neutral species. OrbMol²²⁻²⁴ represents the other extreme, offering high accuracy and coverage of the full OMol25 dataset, spanning most of the periodic table and diverse charge states. AceFF-2 occupies a strategic position between these extremes on the Pareto front; it creates a balance similar in speed and applicability to AIMNet2,¹⁴ yet offers superior accuracy.

The TensorNet2 architecture further extends the expressivity of TensorNet and remains one of the fastest equivariant MLIPs available. The models we have primarily compared

against are invariant (OrbMol, ANI2x, AIMNet2), these are design choices that may have been influenced by the typically higher speed of invariant models²³ when compared to equivariant ones. The only other equivariant model we test is MACE-MPA-0 which is significantly slower. We have not investigated direct force prediction MLIPs (i.e., where forces are output in the forward pass and not by back-propagation) as the inherently non-conservative nature adds significant complexity in using them for stable MD simulations.⁵⁵

AceFF-2 demonstrates substantial improvements over traditional molecular mechanics force fields and our model’s predecessors. Importantly, it supports all standard drug-relevant elements and exhibits strong transferability to larger, out-of-distribution molecules. The model produces stable molecular dynamics trajectories for both in-vacuum simulations and hybrid MLIP/MM protein-ligand systems.

AceFF-2 is available to the community, supported by code and tutorials to enable rapid adoption within both the ASE and OpenMM-ML frameworks. We anticipate that AceFF-2 will facilitate more accurate and computationally tractable molecular simulations, particularly within drug discovery and chemical research, by providing a reliable alternative to classical force fields and computationally expensive quantum calculations. Furthermore, the benchmarks established in this work provide the community with a rigorous new protocol for testing MLIPs.

4 Methods

4.1 Dataset

We built an in-house dataset of DFT data for drug-like small molecules, comprising approximately 2 million unique molecules from PubChem⁵⁶ with 12 million conformations. The elements included are H, B, C, N, O, F, Si, P, S, Cl, Br, and I. Molecule sizes are up to 30 atoms. Charge values include [-2,-1,0,1,2]. The DFT level of theory is ω B97M-V/def2-TZVPPD.⁵⁷ PySCF⁵⁸ and the plugin GPU4PySCF^{59,60} was used. The dataset includes energy-minimized

structures and high-energy geometries. One reason for creating this dataset was the inadequacy of the existing datasets at the time, notably, they did not contain the higher energy structures we believed were necessary for stable MLIPs. We note that OMol25²⁵ has recently been released, which contains 100M conformations, marking a step change in the availability of molecular DFT data.

4.2 Models and force fields

We used ANI2x¹⁷ from TorchANI.⁴³ For all evaluations excluding the OpenMM-based ones, we used the latest TorchANI-2⁴⁹ (version 2.6) For the OpenMM-based simulation, we used an older version (2.2.4,) which is compatible with the NNPOps⁶¹ (version 0.6) package. For OrbMol-conservative²²⁻²⁴ we used version 0.5.5 and all calculations were done via the ASE calculator interface. In the text, we refer to the model as OrbMol-conservative and OrbMol interchangeably. We only ever use the conservative model. For GFN2-XTB³¹ we used version 22.1 from the xtb-python package and used the ASE calculator interface for all evaluations. For g-XTB³⁰ we used the preliminary version 1.1.0 <https://github.com/grimme-lab/g-xtb>. We used GAFF^{1,2} version 2.2 via the OpenMM force-fields package and did all evaluations with OpenMM⁵² version 8.4. For MACE-MPA-0 we used mace-torch version 0.3.14 and the MPA-0 foundation model.⁶² For UMA-s-1.2 we used the omol task from fairchem-core version 2.17. We used ASE⁴⁸ version 3.26. We used OpenMM-ML version 1.2, OpenMM-Torch version 1.5, and OpenMM version 8.4.

Some models have specific limitations and were therefore excluded from certain tests. ANI2x supports only elements H, C, N, O, S, F, and Cl. g-XTB lacks analytical gradients, so we did not use it for tests requiring force calculations. OrbMol is not TorchScript compatible, so we could not use it with the OpenMM/OpenMM-Torch/OpenMM-ML interface. Additionally, the current OpenMM-ML 1.2 release implements only ANI2x and MACE models, so AIMNet2 could not be tested yet. Finally, the MACE-MPA-0 model is designed for materials rather than biomolecules; as its accuracy on these benchmarks would be insufficient

for meaningful comparison, we included it only in the speed benchmarks.

4.3 Torsion scans

For the Sellers et al torsion scan, we performed relaxed torsion scans as done in.⁴¹ We used the GeomeTRIC⁶³ package to perform geometry optimizations with the constrained torsion angles. We took the CCSD(T)/CBS conformation as the starting point for each optimization. To compare with the coupled cluster reference, we computed the relative energy of the torsion scan compared to the minimum energy along the scan. To report a single number from each torsion scan, we computed the mean absolute error of the scan from the reference CCSD(T)/CBS scan (MAE).

For the Behara et al torsion scan we followed the protocol and scripts provided in:⁴⁵ We evaluated the single-point energy of each geometry to calculate the torsion scans. For each torsion scan, we then computed the MAE compared to the reference scan as the difference in the relative energies.

4.4 Molecular dynamics

For the molecular dynamics in section 2.8, we used the ASE dynamics method. The water boxes were created with OpenMM’s `addSolvent` functionality. The MD was run with an artificially small timestep and 100 steps. The timings were recorded every 10 steps and the first values were omitted to ignore the overhead of any PyTorch compilation warmup. The simulations were run on an RTX4090. For the batched molecular dynamics, we used a modified version of the Langevin Integrator from TorchMD.⁵⁰ For the MLIP/MM molecular dynamics in section 2.9 we used a customized version of the OpenMM-ML package along with OpenMM-Torch version 1.5 and OpenMM version 8.4 on an RTX4090. The simulations were run for 100ns with snapshots saved every 10000 steps. The LangevinMiddle integrator was used with a frequency of 1/ps, a temperature of 300K, HMR of 4au, and a timestep of either 1fs or 2fs. For ANI-2x we employed NNPOps.⁶¹ The AceFF simulation was run

using torchmd-net configured with max-num-neighbors=32, and CUDA graphs enabled. For MACE-MPA-0 we used the NNPOps neighbor list.

4.5 Software and data availability

TensorNet2 is available under the MIT license at <https://github.com/torchmd/torchmd-net>. We have provided a set of example IPython notebooks (which can be run on Google Colab) and a Python package containing code to enable using AceFF as an ASE (Atomic Simulation Environment⁴⁸) calculator and in OpenMM-ML⁵² as an ML potential. The package and example notebooks can be found on the GitHub repository https://github.com/Acellera/aceff_examples. The AceFF models can be downloaded from HuggingFace.²⁹ A tutorial to use the models for ML/ML simulations can be found at <https://software.acellera.com/acemd/nnpmm.html>.

Our changes to AIMNet2 for CUDA-graph compatibility can be found in a PR in the main repository <https://github.com/isayevlab/aimnetcentral>.

The dataset for the Wiggle150 benchmark can be found at.⁴⁶ The dataset for the Sellers et al torsion scan can be found at.⁴⁰ The structures for the Schrodinger Ligand set can be found at⁴⁷ and https://github.com/schrodinger/public_binding_free_energy_benchmark. The Behara et al torsion scan data can be found at.⁴⁵ The Platinum Diverse dataset can be found at.⁵³

Author contributions

S.E.F. and G.D.F. wrote the manuscript. S.E.F. implemented the TensorNet2 architecture. S.E.F., S.D., and A.M. developed the AceFF models and datasets. S.E.F and F.S.Z performed the model benchmarks. G.D.F directed the work.

Acknowledgments

The authors thank the volunteers of GPUGRID.net for donating computing time. This project has received funding from the Torres-Quevedo Program from the Spanish National Agency for Research (PTQ2023-012967/AEI/10.13039/501100011033). AM is financially supported by Generalitat de Catalunya’s Agency for Management of University and Research Grants (AGAUR) PhD grant 2025 FI-2-00278.

Competing interests

The authors declare the following competing financial interest(s): S.E.F, S.D, F.S.Z, and G.D.F. have a potential conflict of interest due to direct interests in Acellera (See affiliations).

References

- (1) Wang, J.; Wolf, R. M.; Caldwell, J. W.; Kollman, P. A.; Case, D. A. Development and testing of a general amber force field. *Journal of computational chemistry* **2004**, *25*, 1157–1174.
- (2) Wang, J.; Wang, W.; Kollman, P. A.; Case, D. A. Automatic atom type and bond type perception in molecular mechanical calculations. *J. Mol. Graphics Modell.* **2006**, *25*, 247–260.
- (3) Vanommeslaeghe, K.; Hatcher, E.; Acharya, C.; Kundu, S.; Zhong, S.; Shim, J.; Darian, E.; Guvench, O.; Lopes, P.; Vorobyov, A., Igor MacKerell Jr CHARMM general force field: A force field for drug-like molecules compatible with the CHARMM all-atom additive biological force fields. *Journal of computational chemistry* **2010**, *31*, 671–690.
- (4) Vanommeslaeghe, K.; Raman, E. P.; MacKerell Jr, A. D. Automation of the CHARMM

- General Force Field (CGenFF) II: assignment of bonded parameters and partial atomic charges. *Journal of chemical information and modeling* **2012**, *52*, 3155–3168.
- (5) Qiu, Y.; Smith, D. G.; Boothroyd, S.; Jang, H.; Hahn, D. F.; Wagner, J.; Bannan, C. C.; Gokey, T.; Lim, V. T.; Stern, C. D.; others Development and benchmarking of open force field v1. 0.0—the parsley small-molecule force field. *Journal of chemical theory and computation* **2021**, *17*, 6262–6280.
- (6) Boothroyd, S.; Behara, P. K.; Madin, O. C.; Hahn, D. F.; Jang, H.; Gapsys, V.; Wagner, J. R.; Horton, J. T.; Dotson, D. L.; Thompson, M. W.; others Development and benchmarking of open force field 2.0. 0: the Sage small molecule force field. *Journal of chemical theory and computation* **2023**, *19*, 3251–3275.
- (7) Maier, J. A.; Martinez, C.; Kasavajhala, K.; Wickstrom, L.; Hauser, K. E.; Simmerling, C. ff14SB: improving the accuracy of protein side chain and backbone parameters from ff99SB. *J. Chem. Theory Comput.* **2015**, *11*, 3696–3713.
- (8) Behler, J.; Parrinello, M. Generalized Neural-Network Representation of High-Dimensional Potential-Energy Surfaces. *Physical Review Letters* **2007**, *98*, 146401.
- (9) Bartók, A. P.; Payne, M. C.; Kondor, R.; Csányi, G. Gaussian Approximation Potentials: The Accuracy of Quantum Mechanics, without the Electrons. *Physical Review Letters* **2010**, *104*, 136403.
- (10) Smith, J. S.; Isayev, O.; Roitberg, A. E. ANI-1: an extensible neural network potential with DFT accuracy at force field computational cost. *Chemical Science* **2017**, *8*, 3192–3203.
- (11) Unke, O. T.; Chmiela, S.; Sauceda, H. E.; Gastegger, M.; Poltavsky, I.; Schütt, K. T.; Tkatchenko, A.; Müller, K.-R. Machine Learning Force Fields. *Chemical Reviews* **2021**, *121*, 10142–10186.

- (12) Batatia, I.; Kovács, D. P.; Simm, G. N. C.; Ortner, C.; Csányi, G. MACE: Higher Order Equivariant Message Passing Neural Networks for Fast and Accurate Force Fields. 2023; <http://arxiv.org/abs/2206.07697>, arXiv:2206.07697.
- (13) Batzner, S.; Musaelian, A.; Sun, L.; Geiger, M.; Mailoa, J. P.; Kornbluth, M.; Molinari, N.; Smidt, T. E.; Kozinsky, B. E(3)-equivariant graph neural networks for data-efficient and accurate interatomic potentials. *Nature Communications* **2022**, *13*, 2453.
- (14) Anstine, D.; Zubatyuk, R.; Isayev, O. AIMNet2: a neural network potential to meet your neutral, charged, organic, and elemental-organic needs. *Chemrxiv preprint chemrxiv-2023-296ch-v3* **2024**,
- (15) Simeon, G.; De Fabritiis, G. TensorNet: Cartesian Tensor Representations for Efficient Learning of Molecular Potentials. *Advances in Neural Information Processing Systems*. 2023; pp 37334–37353.
- (16) Duval, A.; Mathis, S. V.; Joshi, C. K.; Schmidt, V.; Miret, S.; Malliaros, F. D.; Cohen, T.; Lio, P.; Bengio, Y.; Bronstein, M. A Hitchhiker’s Guide to Geometric GNNs for 3D Atomic Systems. *arXiv preprint arXiv:2312.07511* **2023**,
- (17) Devereux, C.; Smith, J. S.; Huddleston, K. K.; Barros, K.; Zubatyuk, R.; Isayev, O.; Roitberg, A. E. Extending the Applicability of the ANI Deep Learning Molecular Potential to Sulfur and Halogens. *Journal of Chemical Theory and Computation* **2020**, *16*, 4192–4202, PMID: 32543858.
- (18) Kovács, D. P.; Moore, J. H.; Browning, N. J.; Batatia, I.; Horton, J. T.; Kapil, V.; Witt, W. C.; Magdău, I.-B.; Cole, D. J.; Csányi, G. MACE-OFF23: Transferable machine learning force fields for organic molecules. *arXiv preprint arXiv:2312.15211* **2023**,
- (19) Acellera AceFF-1.0 on HuggingFace. <https://huggingface.co/Acellera/AceFF-1.0>, 2024; Accessed: 2025-02-24.

- (20) Simeon, G.; Mirarchi, A.; Pelaez, R. P.; Galvelis, R.; De Fabritiis, G. Broadening the Scope of Neural Network Potentials through Direct Inclusion of Additional Molecular Attributes. *Journal of Chemical Theory and Computation* **2025**, *21*, 1831–1837.
- (21) Mann, E. L.; Wagen, C. C.; Vandezande, J. E.; Wagen, A. M.; Schneider, S. C. Egret-1: Pretrained Neural Network Potentials For Efficient and Accurate Bioorganic Simulation. 2025; <https://arxiv.org/abs/2504.20955>.
- (22) Materials, O. OrbMol. <https://huggingface.co/Orbital-Materials/OrbMol>, 2025; Hugging Face repository. Accessed: 2025-11-17.
- (23) Rhodes, B.; Vandenhaute, S.; Šimkus, V.; Gin, J.; Godwin, J.; Duignan, T.; Neumann, M. Orb-v3: atomistic simulation at scale. 2025; <https://arxiv.org/abs/2504.06231>.
- (24) Neumann, M.; Gin, J.; Rhodes, B.; Bennett, S.; Li, Z.; Choubisa, H.; Hussey, A.; Godwin, J. Orb: A Fast, Scalable Neural Network Potential. 2024; <http://arxiv.org/abs/2410.22570>, arXiv:2410.22570.
- (25) Levine, D. S.; Shuaibi, M.; Spotte-Smith, E. W. C.; Taylor, M. G.; Hasyim, M. R.; Michel, K.; Batatia, I.; Csányi, G.; Dzamba, M.; Eastman, P.; Frey, N. C.; Fu, X.; Gharakhanyan, V.; Krishnapriyan, A. S.; Rackers, J. A.; Raja, S.; Rizvi, A.; Rosen, A. S.; Ulissi, Z.; Vargas, S.; Zitnick, C. L.; Blau, S. M.; Wood, B. M. The Open Molecules 2025 (OMol25) Dataset, Evaluations, and Models. 2025; <https://arxiv.org/abs/2505.08762>.
- (26) Kabylda, A.; Frank, J. T.; Suárez-Dou, S.; Khabibrakhmanov, A.; Medrano Sandoñas, L.; Unke, O. T.; Chmiela, S.; Müller, K.-R.; Tkatchenko, A. Molecular Simulations with a Pretrained Neural Network and Universal Pairwise Force Fields. *Journal of the American Chemical Society* **2025**, *147*, 33723–33734.

- (27) Sabanéés Zariquiey, F.; Galvelis, R.; Gallicchio, E.; Chodera, J. D.; Markland, T. E.; De Fabritiis, G. Enhancing Protein–Ligand Binding Affinity Predictions Using Neural Network Potentials. *Journal of Chemical Information and Modeling* **2024**, *64*, 1481–1485.
- (28) Sabanéés Zariquiey, F.; Farr, S. E.; Doerr, S.; De Fabritiis, G. QuantumBind-RBFE: Accurate Relative Binding Free Energy Calculations Using Neural Network Potentials. *Journal of Chemical Information and Modeling* **2025**, *65*, 4081–4089.
- (29) Acellera AceForce-1.1 on HuggingFace. <https://huggingface.co/Acellera/AceFF-1.1>, 2025.
- (30) Froitzheim, T.; Müller, M.; Hansen, A.; Grimme, S. g-xTB: A General-Purpose Extended Tight-Binding Electronic Structure Method For the Elements H to Lr (Z=1–103). 2025; <https://chemrxiv.org/engage/chemrxiv/article-details/685434533ba0887c335fc974>.
- (31) Bannwarth, C.; Ehlert, S.; Grimme, S. GFN2-xTB—An Accurate and Broadly Parametrized Self-Consistent Tight-Binding Quantum Chemical Method with Multipole Electrostatics and Density-Dependent Dispersion Contributions. *Journal of Chemical Theory and Computation* **2019**, *15*, 1652–1671.
- (32) H. Brooks, W.; C. Guida, W.; G. Daniel, K. The significance of chirality in drug design and development. *Current topics in medicinal chemistry* **2011**, *11*, 760–770.
- (33) Plé, T.; Adjoua, O.; Benali, A.; Posenitskiy, E.; Villot, C.; Lagardère, L.; Piquemal, J.-P. A Foundation Model for Accurate Atomistic Simulations in Drug Design. *ChemRxiv* **2025**,
- (34) Cheng, B. Latent Ewald summation for machine learning of long-range interactions. *npj Computational Materials* **2025**, *11*, 80.

- (35) Ko, T. W.; Finkler, J. A.; Goedecker, S.; Behler, J. A fourth-generation high-dimensional neural network potential with accurate electrostatics including non-local charge transfer. *Nature Communications* **2021**, *12*, 398.
- (36) Pelaez, R. P.; Simeon, G.; Galvelis, R.; Mirarchi, A.; Eastman, P.; Doerr, S.; Thölke, P.; Markland, T. E.; De Fabritiis, G. TorchMD-Net 2.0: Fast Neural Network Potentials for Molecular Simulations. *Journal of Chemical Theory and Computation* **2024**,
- (37) Ko, T. W.; Deng, B.; Nassar, M.; Barroso-Luque, L.; Liu, R.; Qi, J.; Thakur, A. C.; Mishra, A. R.; Liu, E.; Ceder, G.; Miret, S.; Ong, S. P. Materials Graph Library (MatGL), an open-source graph deep learning library for materials science and chemistry. *npj Computational Materials* **2025**, *11*, 253.
- (38) Ko, T. W.; Nassar, M.; Qi, J.; Miret, S.; Ong, S. P. MatGL: Graph deep learning library for materials. 2025; <https://github.com/materializeai/matgl>.
- (39) Semelak, J. A.; Pickering, I.; Huddleston, K.; Olmos, J.; Grassano, J. S.; Clemente, C. M.; Drusin, S. I.; Marti, M.; Gonzalez Lebrero, M. C.; Roitberg, A. E.; Estrin, D. A. Advancing Multiscale Molecular Modeling with Machine Learning-Derived Electrostatics. *Journal of Chemical Theory and Computation* **2025**, *21*, 5194–5207.
- (40) Sellers, B. D.; James, N. C.; Gobbi, A. A comparison of quantum and molecular mechanical methods to estimate strain energy in druglike fragments. *Journal of chemical information and modeling* **2017**, *57*, 1265–1275.
- (41) Smith, J. S.; Nebgen, B. T.; Zubatyuk, R.; Lubbers, N.; Devereux, C.; Barros, K.; Tretiak, S.; Isayev, O.; Roitberg, A. E. Approaching coupled cluster accuracy with a general-purpose neural network potential through transfer learning. *Nature Communications* **2019**, *10*, 2903.
- (42) Smith, J. S.; Roitberg, A. E.; Isayev, O. Transforming Computational Drug Discovery with Machine Learning and AI. *ACS Medicinal Chemistry Letters* **2018**, *9*, 1065–1069.

- (43) Gao, X.; Ramezanghorbani, F.; Isayev, O.; Smith, J. S.; Roitberg, A. E. TorchANI: a free and open source PyTorch-based deep learning implementation of the ANI neural network potentials. *Journal of chemical information and modeling* **2020**, *60*, 3408–3415.
- (44) Bannwarth, C.; Ehlert, S.; Grimme, S. GFN2-xTB—An accurate and broadly parametrized self-consistent tight-binding quantum chemical method with multipole electrostatics and density-dependent dispersion contributions. *Journal of chemical theory and computation* **2019**, *15*, 1652–1671.
- (45) Behara, P. K.; Jang, H.; Horton, J. T.; Gokey, T.; Dotson, D. L.; Boothroyd, S.; Bayly, C. I.; Cole, D. J.; Wang, L.-P.; Mobley, D. L. Benchmarking Quantum Mechanical Levels of Theory for Valence Parametrization in Force Fields. *The Journal of Physical Chemistry B* **2024**, *128*, 7888–7902, PMID: 39087913.
- (46) Brew, R.; Nelson, I.; Binayeva, M.; Nayak, A.; Simmons, W.; Gair, J.; Wagen, C. Wiggle150: Benchmarking Density Functionals And Neural Network Potentials On Highly Strained Conformers. 2025; <https://chemrxiv.org/engage/chemrxiv/article-details/67f5035c6dde43c908ee4655>.
- (47) Ross, G. A.; Lu, C.; Scarabelli, G.; Albanese, S. K.; Houang, E.; Abel, R.; Harder, E. D.; Wang, L. The maximal and current accuracy of rigorous protein-ligand binding free energy calculations. *Communications Chemistry* **2023**, *6*, 222.
- (48) Hjorth Larsen, A.; Jørgen Mortensen, J.; Blomqvist, J.; Castelli, I. E.; Christensen, R.; Dułak, M.; Friis, J.; Groves, M. N.; Hammer, B.; Hargus, C.; Hermes, E. D.; Jennings, P. C.; Bjerre Jensen, P.; Kermode, J.; Kitchin, J. R.; Leonhard Kolsbjerg, E.; Kubal, J.; Kaasbjerg, K.; Lysgaard, S.; Bergmann Maronsson, J.; Maxson, T.; Olsen, T.; Pastewka, L.; Peterson, A.; Rostgaard, C.; Schiøtz, J.; Schütt, O.; Strange, M.; Thygesen, K. S.; Vegge, T.; Vilhelmsen, L.; Walter, M.; Zeng, Z.; Jacob-

- sen, K. W. The atomic simulation environment—a Python library for working with atoms. *Journal of Physics: Condensed Matter* **2017**, *29*, 273002.
- (49) Pickering, I.; Xue, J.; Huddleston, K.; Terrel, N.; Roitberg, A. E. TorchANI 2.0: An Extensible, High-Performance Library for the Design, Training, and Use of NN-IPs. *Journal of Chemical Information and Modeling* **2025**, *65*, 11656–11671.
- (50) Doerr, S.; Majewski, M.; Pérez, A.; Kramer, A.; Clementi, C.; Noe, F.; Giorgino, T.; De Fabritiis, G. TorchMD: A deep learning framework for molecular simulations. *Journal of chemical theory and computation* **2021**, *17*, 2355–2363.
- (51) Rufa, D. A.; Macdonald, H. E. B.; Fass, J.; Wieder, M.; Grinaway, P. B.; Roitberg, A. E.; Isayev, O.; Chodera, J. D. Towards chemical accuracy for alchemical free energy calculations with hybrid physics-based machine learning / molecular mechanics potentials. *bioRxiv* **2020**,
- (52) Eastman, P.; Galvelis, R.; Peláez, R. P.; Abreu, C. R.; Farr, S. E.; Gallicchio, E.; Gorenko, A.; Henry, M. M.; Hu, F.; Huang, J.; others OpenMM 8: molecular dynamics simulation with machine learning potentials. *The Journal of Physical Chemistry B* **2023**, *128*, 109–116.
- (53) Friedrich, N.-O.; Meyder, A.; de Bruyn Kops, C.; Sommer, K.; Flachsenberg, F.; Rarey, M.; Kirchmair, J. High-Quality Dataset of Protein-Bound Ligand Conformations and Its Application to Benchmarking Conformer Ensemble Generators. *Journal of Chemical Information and Modeling* **2017**, *57*, 529–539, PMID: 28206754.
- (54) National Center for Biotechnology Information PubChem Compound Summary for CID 5291, Imatinib. <https://pubchem.ncbi.nlm.nih.gov/compound/Imatinib>, 2025; Retrieved November 18, 2025.
- (55) Bigi, F.; Langer, M.; Ceriotti, M. The dark side of the forces: assessing non-conservative

- force models for atomistic machine learning. 2025; <https://arxiv.org/abs/2412.11569>.
- (56) Kim, S.; Chen, J.; Cheng, T.; Gindulyte, A.; He, J.; He, S.; Li, Q.; Shoemaker, B.; Thiessen, P.; Yu, B.; Zaslavsky, L.; Zhang, J.; Bolton, E. PubChem 2025 update. *Nucleic Acids Research* **2025**, *53*, D1516–D1525.
- (57) Mardirossian, N.; Head-Gordon, M. ω B97M-V: A combinatorially optimized, range-separated hybrid, meta-GGA density functional with VV10 nonlocal correlation. *The Journal of Chemical Physics* **2016**, *144*, 214110.
- (58) Sun, Q.; Zhang, X.; Banerjee, S.; Bao, P.; Barbry, M.; Blunt, N. S.; Bogdanov, N. A.; Booth, G. H.; Chen, J.; Cui, Z.-H.; Eriksen, J. J.; Gao, Y.; Guo, S.; Hermann, J.; Hermes, M. R.; Koh, K.; Koval, P.; Lehtola, S.; Li, Z.; Liu, J.; Mardirossian, N.; McClain, J. D.; Motta, M.; Mussard, B.; Pham, H. Q.; Pulkin, A.; Purwanto, W.; Robinson, P. J.; Ronca, E.; Sayfutyarova, E. R.; Scheurer, M.; Schurkus, H. F.; Smith, J. E. T.; Sun, C.; Sun, S.-N.; Upadhyay, S.; Wagner, L. K.; Wang, X.; White, A.; Whitfield, J. D.; Williamson, M. J.; Wouters, S.; Yang, J.; Yu, J. M.; Zhu, T.; Berkelbach, T. C.; Sharma, S.; Sokolov, A. Y.; Chan, G. K.-L. Recent developments in the PySCF program package. *The Journal of Chemical Physics* **2020**, *153*, 024109.
- (59) Li, R.; Sun, Q.; Zhang, X.; Chan, G. K.-L. Introducing GPU-acceleration into the Python-based Simulations of Chemistry Framework. 2024; <https://arxiv.org/abs/2407.09700>.
- (60) Wu, X.; Sun, Q.; Pu, Z.; Zheng, T.; Ma, W.; Yan, W.; Yu, X.; Wu, Z.; Huo, M.; Li, X.; Ren, W.; Gong, S.; Zhang, Y.; Gao, W. Enhancing GPU-acceleration in the Python-based Simulations of Chemistry Framework. 2024; <https://arxiv.org/abs/2404.09452>.
- (61) Galvelis, R.; Varela-Rial, A.; Doerr, S.; Fino, R.; Eastman, P.; Markland, T. E.;

- Chodera, J. D.; De Fabritiis, G. NNP/MM: Accelerating molecular dynamics simulations with machine learning potentials and molecular mechanics. *Journal of chemical information and modeling* **2023**, *63*, 5701–5708.
- (62) Batatia, I.; Benner, P.; Chiang, Y.; Elena, A. M.; Kovács, D. P.; Riebesell, J.; Advincula, X. R.; Asta, M.; Baldwin, W. J.; Bernstein, N.; Bhowmik, A.; Blau, S. M.; Cărare, V.; Darby, J. P.; De, S.; Pia, F. D.; Deringer, V. L.; Elijošius, R.; Elmachachi, Z.; Fako, E.; Ferrari, A. C.; Genreith-Schriever, A.; George, J.; Goodall, R. E. A.; Grey, C. P.; Han, S.; Handley, W.; Heenen, H. H.; Hermansson, K.; Holm, C.; Jaafar, J.; Hofmann, S.; Jakob, K. S.; Jung, H.; Kapil, V.; Kaplan, A. D.; Karimitari, N.; Kroupa, N.; Kullgren, J.; Kuner, M. C.; Kuryla, D.; Liepuoniute, G.; Margraf, J. T.; Magdău, I.-B.; Michaelides, A.; Moore, J. H.; Naik, A. A.; Niblett, S. P.; Norwood, S. W.; O'Neill, N.; Ortner, C.; Persson, K. A.; Reuter, K.; Rosen, A. S.; Schaaf, L. L.; Schran, C.; Sivonxay, E.; Stenczel, T. K.; Svahn, V.; Sutton, C.; van der Oord, C.; Varga-Umbrich, E.; Vegge, T.; Vondrák, M.; Wang, Y.; Witt, W. C.; Zills, F.; Csányi, G. A foundation model for atomistic materials chemistry. **2023**,
- (63) Wang, L.-P.; Song, C. Geometry optimization made simple with translation and rotation coordinates. *The Journal of chemical physics* **2016**, *144*.